Aalborg Universitet

A Simple Space Vector Modulation of High-Frequency AC Linked Three-Phase-to-Single-Phase/DC Converter

Liu, Yushan; He, Jie; Ge, Baoming; Li, Xiao; Xue, Yaosuo; Blaabjerg, Frede

A Simple Space Vector Modulation of High-Frequency AC Linked Three-Phase-to-Single-Phase/DC Converter

YUSHAN LIU[1], (Senior Member, IEEE), **JIE HE**[1], **BAOMING GE**[2], (Member, IEEE),
XIAO LI[2], (Member, IEEE), **YAOSUO XUE**[3], (Senior Member, IEEE),
AND FREDE BLAABJERG[4], (Fellow, IEEE)

[1]School of Automation Science and Electrical Engineering, Beihang University, Beijing 100083, China
[2]Department of Electrical and Computer Engineering, Texas A&M University, College Station, TX 77843, USA
[3]Oak Ridge National Laboratory, Oak Ridge, TN 37831, USA
[4]Department of Energy Technology, Aalborg University, 9220 Aalborg, Denmark

Corresponding author: Xiao Li (xiaoli.tamu@gmail.com)

ABSTRACT High frequency (HF) ac linked converter functions well to interface between buses with different voltage types. Using a three-phase-to-single-phase matrix converter, a single-phase cyclo converter, and a HF transformer, we can compose a HF ac linked converter to interface between three-phase ac grids and single-phase ac or dc distributed generations (DGs). In this paper, a novel space vector modulation (SVM) method is proposed for such kind of converter. The proposed SVM method converts the mains three-phase ac voltage to a HF ac voltage at the primary side of transformer, and then unfolds the HF ac voltage to a single-phase ac or dc voltage at the secondary side of transformer. Without need to compute separate switching signals for the primary and secondary converters and then coordinate their operations elaborately, the proposed SVM method can be easily implemented by incorporating the HF chopping into the SVM of traditional indirect matrix converter. Therefore, no complicated duty cycle computation or elaborate switching states combination is required. Simulation and hardware-in-loop implementation demonstrate the validity of the proposed method.

INDEX TERMS High-frequency ac, matrix converter, space vector modulation, distributed generations.

I. INTRODUCTION

The high-frequency (HF) ac linked converters, known as smart transformers, are playing a crucial role in the ever-increasing demand for smarter energy management, due to the growing penetration of distributed generations (DGs) [1]–[4]. The traditional line-frequency (LF) transformer is extremely bulky, expensive, uncontrollable, and vulnerable to power quality issues. Therefore, increasing interests are dedicated to the smart transformers, which are well known for HF operation and high controllability [4]–[6]. The high operating frequency at tens of kilo Hertz significantly reduces transformer sizes and consequently distribution system volumes and weights. The high controllability empowers functions

such as power factor correction, voltage regulation, fault tolerance, etc., compared to the traditional LF transformer.

The dual-active-bridge (DAB) converter-based smart transformer consists of two H-bridge converters linked through a HF ac transformer, which can easily incorporate renewable energy sources and energy storage devices due to the presence of low-voltage dc link [7]–[10]. In case the DAB needs to be connected with utility grids, a front-end active rectifier is used to convert the three-phase ac to dc, usually as a high-voltage dc link of system [11]. Electrolytic capacitor banks are often required at both high-voltage and low-voltage dc links in such a two-stage system for energy storage purpose. The bulky failure prone dc-link capacitors not only contradict with compact volume, but also decrease the system lifespan and reliability. The single-stage matrix converter-type HF ac linked converter is another

The associate editor coordinating the review of this manuscript and approving it for publication was Jenny Mahoney.

TABLE 1. Performance of typical HF ac linked converters.

	Input	Output	Switch count	Storage Elements	Reliability	Volume	Stackable to high power
Dual-active-bridge converter, [7]-[10]	dc	dc	Single switch in each bridge arm, totally 8	Electrolytic capacitor banks	Low	Bulky	Yes
Dual-active-bridge converter with front-end active rectifier, [11]	Three-phase ac	dc	Single switch in each bridge arm, totally 14	Electrolytic capacitor banks	Low	Bulky	Yes
Three-phase-to-single-phase matrix converter and one-leg cyclo converter of each phase, [12]	Three-phase ac	Three-phase ac	Two back-to-back switches in each bridge arm, totally 48	Not required	High	Compact	Yes
Two three-phase-to-single-phase matrix converters in back-to-back HF ac linking, [13]-[16]	Three-phase ac	Three-phase ac	Two back-to-back switches in each bridge arm, totally 24	Not required	High	Compact	No
Three-to-single-phase matrix converter and diode bridge formed isolated rectifier, [22]-[25]	Three-phase ac	dc	Two back-to-back switches in 6 arms, totally 12 switches and 4 diodes	Not required	High	Compact	No
Three-to-single-phase matrix converter and active-bridge converter formed isolated rectifier, [26]-[30]	Three-phase ac	dc	Two back-to-back switches in 6 arms and single switch in 4 arms, totally 16	Not required	High	Compact	No
Dual single-phase cyclo converters module of each phase, [31]	Three-phase ac	Single-phase ac	Two back-to-back switches in each bridge arm, totally 48 in case of three modules in cascade.	Not required	High	Compact	Yes
Three-to-single-phase matrix converter and single-phase cyclo converter, [32]	Three-phase ac	dc or single-phase ac	Two back-to-back switches in each bridge arm, totally 20	Not required	High	Compact	Yes

solution [12]–[32]. As a single-stage converter, it is able to convert ac voltage amplitude and/or frequency directly without the need of intermediate electrolytic capacitors. In addition to the inherited characteristics from traditional matrix converters [33]–[39], high reliability and compact volume are achievable [12], [22], [23], [28]–[31], [34].

The matrix converter-type smart transformer formed by three-phase-to-single-phase (TPSP) matrix converter and one-leg cyclo converter of each phase dims its attraction due to the fact of large switch counts and complicated modulation [12]. That is then improved by back-to-back linking of two TPSP matrix converters [13], which has gained particular attentions due to its simple structure and reduced switch count [14]–[16]. The bidirectional bridge arm of that kind of HF ac linked converter replaced by the IGBT in series with a diode or reverse-blocking IGBT, as called dynamic current (Dyna-C) topology [17], allows current to conduct in only one direction but blocks voltages in both directions. Soft-switching technique, high-power prototype design, and a class of partial resonant ac-link topology are developed [18]–[21]. The above matrix converter-type smart transformers mainly interface the three-phase ac with three-phase ac. In applications where a converting interface between utility grids and dc loads or sources, such as

vehicle-to-grid (V2G), the TPSP matrix converter linking a diode bridge or active bridge would be useful [22]–[30]. A TPSP matrix converter with an active rectifier bridge is reported with a 99% efficiency using modern silicon carbide (SiC) devices [29], which is very attractive for such applications. In order to have modularity in high-power applications while improving controllability in unbalanced grid conditions, dual single-phase cyclo converters linked in HF ac are developed as a module of each phase forming three-phase smart transformer. That converter has the characteristics of matrix converter, especially the high flexibility, and can be easily scaled to operate in high power conditions owing to the single-phase module-based structure [31]. Furthermore, the TPSP matrix converter and single-phase cyclo converter linked through HF ac, which is going to be investigated in this paper, functions well to convert three-phase ac to single-phase ac or dc, vise versa. That makes it particularly attractive for future distribution grids as a universal interface between the mains grid and DGs [32], [37]. Besides all advantages of matrix converter-type smart transformers, it also allows the single-phase side cyclo converter to be stacked for high-voltage and high-power operations, resulting in much less switch count than single-phase cyclo converter modules formed one in [31]. As a summary, Table 1 lists the

performances of the above discussed typical HF ac linked converters.

The modulation method of HF ac linked converter needs to deal with the voltage and current control of primary and secondary converters simultaneously, as well as the power flow, current commutation, and leakage energy management, because of the coupling. Therewith, the duty cycle implementation-based space vector modulation (SVM) is a good choice to achieve those goals [40]. An SVM was proposed for the back-to-back TPSP matrix converter-type smart transformers, which is complicated due to computing the duty cycles of the two TPSP matrix converters, respectively, and then combining the two parts in an elaborate way [12], [13]. An indirect SVM was proposed in order to simplify the implementation [14], [15], but with three-phase ac on both sides. Model predictive control was developed for that kind of HF ac linked converter, which brings the features of simple control structure and fast responses [16], [41], but with variable switching frequency challenging the prototype design. A general SVM was proposed for the TPSP matrix converter and single-phase cyclo converter formed HF ac converter interfacing three-phase ac with single-phase ac or dc, whereas, detailed analysis of circuit operation or hardware implementation was not provided [32]. So far, there has been no other SVM developed for this kind of HF ac converter.

This paper proposes an SVM method for the TPSP matrix converter and single-phase cyclo converter formed smart transformer, which can be used to interface the three-phase ac with single-phase ac or dc DGs bidirectionally. This kind of modulation method is easy to implement by incorporating the HF chopping into the SVM of traditional indirect matrix converter (IMC) in a novel way as the first time, without computing separate switching signals for the primary and secondary converters and then coordinating the operations in an elaborate way as done. Simulation and hardware-in-loop (HIL) results are demonstrated to verify the proposed method. The paper is structured as follows: Section II introduces the discussed HF ac linked converter; Section III details the proposed SVM and analyzes operating modes; Section IV illustrates simulation studies and HIL implementation; finally, Section V concludes the work.

II. HF AC LINKED THREE-PHASE-TO-SINGLE-PHASE/DC CONVERTER

Fig. 1 shows the HF ac linked converter interfacing three-phase ac grid with single-phase ac or dc DGs. The primary side is a TPSP matrix converter, converting the three-phase ac to HF ac voltage. The secondary side is a single-phase cyclo converter obtaining single-phase ac or dc voltage for the DGs. The two converters are linked through an n_1: n_2 HF transformer. In this way, the three-phase ac power source could be converted to either supply a single-phase ac/dc load or tie directly to single-phase ac/dc grid. As a bidirectional configuration, it can also be used to interface a single-phase ac grid or dc grid with the three-phase power source/loads.

The three-phase side is denoted as the transformer primary in the following illustration.

The switch of each bridge arm in the matrix converter and cyclo converter could be a bidirectional switch, such as two back-to-back connected switches, an IGBT in series with a diode, or a reverse-blocking IGBT [17]–[21]. Here, the general back-to-back connected switch is used for illustration purpose.
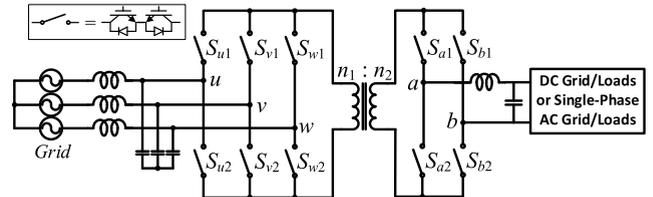

FIGURE 1. Topology of discussed HF ac linked converter interfacing three-phase ac grid with single-phase ac or dc DGs.

As shown in Fig. 1, the matrix converter consists of six bidirectional power switches, named as S_{ij}, $i \in \{u, v, w\}$ for the three phases and $j \in \{1, 2\}$ for the upper and lower bridges. The cyclo converter is with four bidirectional switches S_{mj}, $m \in \{a, b\}$ for the two phases.

Fig. 2 shows the equivalent operating circuit of this HF ac linked converter, where a virtual DAB represents the HF transformer. Denote the primary and secondary sides switches of DAB with $S_1 \sim S_4$ and $S_5 \sim S_8$, respectively.

At the primary side, the TPSP matrix converter in Fig. 1 is equivalent to a current source rectifier with a virtual active-bridge inverter. The three-phase input voltages $u_{in\{u,v,w\}}$ of the matrix converter are rectified into a virtual dc voltage V_{dc1}, which is then chopped to HF ac voltage v_p by the virtual active-bridge inverter. Denote the switches of the equivalent rectifier in Fig. 2 as S'_{ij}. The operation of primary TPSP matrix converter in Fig. 1 could be written as

$$\begin{bmatrix} S_{u1} & S_{v1} & S_{w1} \\ S_{u2} & S_{v2} & S_{w2} \end{bmatrix} = \begin{bmatrix} S_1 & S_2 \\ S_3 & S_4 \end{bmatrix} \begin{bmatrix} S'_{u1} & S'_{v1} & S'_{w1} \\ S'_{u2} & S'_{v2} & S'_{w2} \end{bmatrix} \quad (1)$$

The v_p is then transferred to the secondary side at v_s through the n_1: n_2 HF transformer. The secondary cyclo converter is equivalent to a virtual active-bridge converter in series with a H-bridge inverter. The virtual active-bridge converter firstly recovers the virtual dc-link voltage V_{dc2} from the HF ac voltage v_s, then unfolds the V_{dc2} to the single-phase ac or adjustable dc voltage by H-bridge switches S'_{mj}. Hence, the operation of secondary cyclo converter is equal to

$$\begin{bmatrix} S_{a1} & S_{b1} \\ S_{a2} & S_{b2} \end{bmatrix} = \begin{bmatrix} S_5 & S_6 \\ S_7 & S_8 \end{bmatrix} \begin{bmatrix} S'_{a1} & S'_{b1} \\ S'_{a2} & S'_{b2} \end{bmatrix} \quad (2)$$

III. PROPOSED SVM OF THE HF AC LINKED CONVERTER

In Fig. 2, if we observe from the secondary side and remove the virtual DAB converter, the circuit can be seen as an IMC, formed by rectifier stage switches S'_{ij} and inversion stage switches S'_{mj}. According to (1) and (2), the switching actions
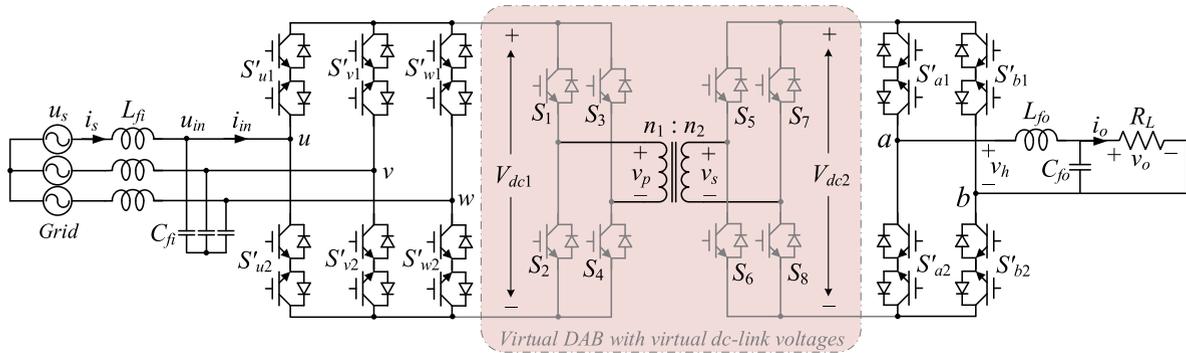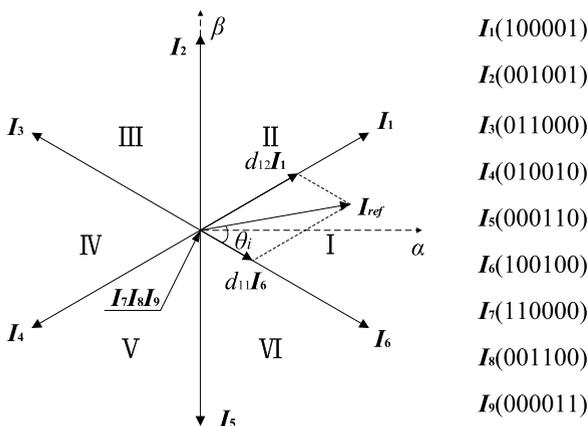
FIGURE 2. Equivalent operating circuit of the discussed HF ac linked converter.

of S'_{ij} and S'_{mj} combining that of the virtual DAB can produce those for the S_{ij} and S_{mj}.

Hence, through the SVM of conventional IMC and HF chop of DAB converter, a simple to implement SVM is proposed for the HF ac linked converter in Fig. 1. Accordingly, the method would follow through two steps: 1) selecting switching states and calculating duty cycles of rectifier and inversion stages based on that for conventional IMC, except that the inversion stage is single-phase ac/dc voltage; 2) combining duty cycles and implementing switching states considering the HF ac chopping, current commutation, and leakage inductance management. The power flow from three-phase side to single-phase side is illustrated as an example, which can be inherited for a reverse power flow.

A. SWITCHING STATES SELECTION AND DUTY CYCLES CALCULATION

According to the SVM of a conventional IMC, Fig. 3 shows the current space vectors of the rectifier stage. There are nine current vectors, including six active vectors ($I_1 \sim I_6$) and three zero vectors ($I_7 \sim I_9$). The active vectors divide the space into six sectors I~VI. When falling into any

$I_1(100001)$
$I_2(001001)$
$I_3(011000)$
$I_4(010010)$
$I_5(000110)$
$I_6(100100)$
$I_7(110000)$
$I_8(001100)$
$I_9(000011)$

*Example: $I_1(100001)$ denotes
S'_{u1}=ON, S'_{u2}=OFF, S'_{v1}=OFF, S'_{v2}=OFF, S'_{w1}=OFF, S'_{w2}=ON.

FIGURE 3. Diagram of rectifier-stage current space vectors.

*Example: $V_1(1001)$ denotes
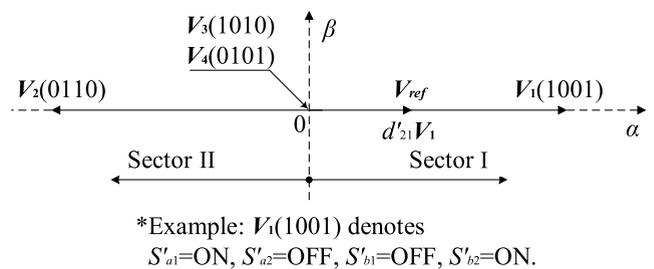S'_{a1}=ON, S'_{a2}=OFF, S'_{b1}=OFF, S'_{b2}=ON.

FIGURE 4. Diagram of inversion-stage voltage space vectors.

sector, the current reference vector I_{ref} are synthesized by the two adjacent active vectors and one of the three zero vectors.

The duty cycles d_{11}, d_{12}, and d_{10} of the two active states and zero state are expressed as [42]

$$d_{11} = M_1 \sin(\pi/3 - \theta_i)$$
$$d_{12} = M_1 \sin(\theta_i)$$
$$d_{10} = 1 - (d_{11} + d_{12}) \quad (3)$$

where $M_1 = I_{ref}/I_p = I_{sm}/I_p$ denotes the modulation index of the equivalent IMC rectifier stage, I_p denotes the absolute value of transformer primary current, I_{sm} denotes the amplitude of three-phase source current, and θ_i denotes the angle of I_{ref} in the *i*th sector.

The SVM of a conventional single-phase inverter [43] is applied to the inversion stage of the equivalent IMC. Fig. 4 shows the voltage space vectors, comprising two active vectors, V_1 and V_2, and two zero vectors, V_3 and V_4. Duty cycles d'_{21} and d'_{20} of the active and zero states in sector I are expressed as

$$d'_{21} = M_2 = V_{ref}/V_{dc2}$$
$$d'_{20} = 1 - d'_{21} \quad (4)$$

where M_2 is the modulation index of the equivalent IMC inversion stage. The M_2 will be $2V_{om}/V_{dc2}$ or V_{om}/V_{dc2} for single-phase ac or dc output. The V_{om} denotes the output voltage amplitude.

B. DUTY CYCLES COMBINATION AND SWITCHING STATES IMPLEMENTATION

To control the primary input current and secondary output voltage simultaneously, the obtained duty cycles of rectifier and inversion stages of the equivalent IMC are firstly combined to consider the current communication and leakage energy management. To achieve that, the inversion stage should keep at zero state to drive the winding current to zero, while the rectifier stage works as normal to build up winding current. Therefore, with (3), the duty cycles of inversion stage in (4) are revised into

$$d_{21} = d'_{21} \cdot d_{11} + d'_{21} \cdot d_{12}$$
$$d_{20} = 1 - d_{21} = 1 - d'_{21}(d_{11} + d_{12})$$
$$= 1 - (1 - d'_{20})(d_{11} + d_{12})$$
$$= d'_{20} \cdot d_{11} + d'_{20} \cdot d_{12} + d_{10} \quad (5)$$

In addition, the switching signals of the virtual DAB $S_1 \sim S_4$ and $S_5 \sim S_8$ alternate in a constant 50% duty cycle at

$$\begin{bmatrix} S_1 & S_2 \\ S_3 & S_4 \end{bmatrix} \in \left\{ \begin{bmatrix} 1 & 0 \\ 0 & 1 \end{bmatrix}, \begin{bmatrix} 0 & 1 \\ 1 & 0 \end{bmatrix} \right\},$$
$$\begin{bmatrix} S_5 & S_6 \\ S_7 & S_8 \end{bmatrix} = \begin{bmatrix} \bar{S}_1 & \bar{S}_2 \\ \bar{S}_3 & \bar{S}_4 \end{bmatrix} \quad (6)$$

which chop the primary virtual dc-link voltage V_{dc1} to the square wave voltage v_p and fold the secondary voltage v_s to the virtual dc-link voltage V_{dc2}.

TABLE 2. Switching states of TPSP matrix converter.

|	Sector v_p Polarity	I	II	III	IV	V	VI
Positive	I_{z1}	I_8	I_7	I_9	I_8	I_7	I_9
	I_a	I_6	I_1	I_2	I_3	I_4	I_5
	I_b	I_1	I_2	I_3	I_4	I_5	I_6
	I_{z2}	I_9	I_8	I_7	I_9	I_8	I_7
Negative	I_{z1}	I_9	I_8	I_7	I_9	I_8	I_7
	I_a	I_4	I_5	I_6	I_1	I_2	I_3
	I_b	I_3	I_4	I_5	I_6	I_1	I_2
	I_{z2}	I_8	I_7	I_9	I_8	I_7	I_9

Then, Table 2 lists all possible switching states of the TPSP matrix converter combined with the HF chopping from the virtual DAB. The I_a and I_b denote the active state vectors to be selected when the reference input current I_{ref} is in the respective sector, I_{z1} and I_{z2} denote the zero state vectors to be used in that sector. Using sector I and positive voltage v_p as an example, as Fig. 3 and Table 2 show, I_6, I_1, I_8, and I_9 are selected for I_a, I_b, I_{z1}, and I_{z2}.

Similarly, Table 3 lists the active state vector V_a and zero state vectors V_{z1} and V_{z2} of the secondary cyclo converter combined with the chopping of virtual DAB.

Thereby, the duty cycles in (3) and (5), with selected switching states in Tables 2 and 3, are utilized to implement the SVM of primary TPSP matrix converter and secondary cyclo converter, respectively, as shown in Figs. 5 and 6.

TABLE 3. Switching states of cyclo converter.

v_s Polarity Sector	Positive			Negative		
	V_{z2}	V_a	V_{z1}	V_{z1}	V_a	V_{z2}
I	V_3	V_1	V_4	V_4	V_2	V_3
II	V_4	V_2	V_3	V_3	V_1	V_4
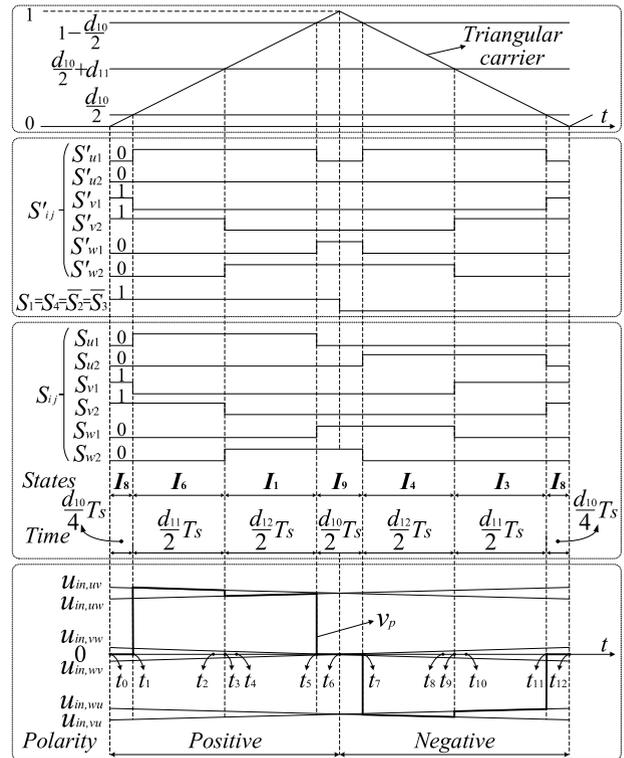
FIGURE 5. Switching states implementation of primary TPSP matrix converter.

Fig. 5 shows the switching states implementation of the primary TPSP matrix converter, when I_{ref} falls in sector I and θ_i is within $\pi/6$. It can be seen that the total zero state duty cycle d_{10} is divided into equal four parts applied in the beginning, middle, and end of one control period. The active state duty cycle d_{11} or d_{12} is equally divided into two parts, applied between the zero and one active state periods. Whereas, from Table 2 and Fig. 5, the rectifier-stage SVM of equivalent IMC is modified through the HF chopping of the virtual DAB, thus, active vectors I_a and I_b are in each half duty cycle of d_{11} and d_{12}, depending on positive or negative v_p. In addition, zero vectors I_{z1} and I_{z2} are also different for the beginning and medium $d_{10}/4$, as well as the medium and last $d_{10}/4$. To maintain minimum switching actions, the same zero vector is applied to the two medium $d_{10}/4$ intervals in one control period, i.e., during the positive and negative transition of v_p.

Fig. 6 shows corresponding implementation of the secondary cyclo converter when V_{ref} is in sector I. Similarly, the inversion-stage SVM of equivalent IMC is modified. Through combining the primary duty cycles in (5) and
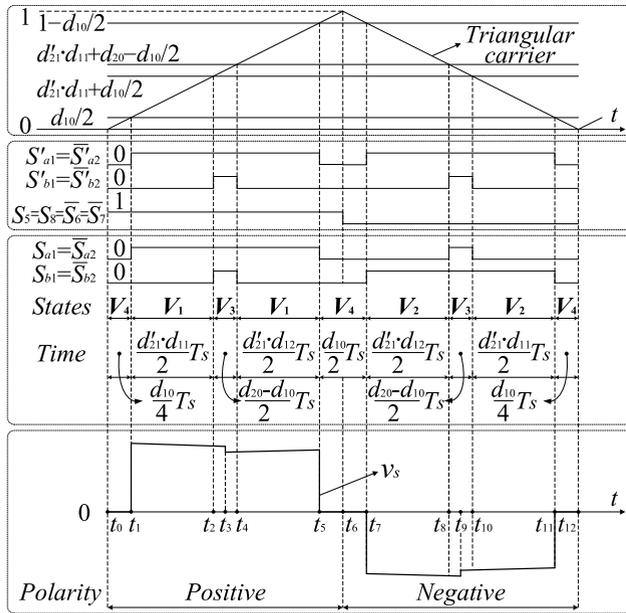
FIGURE 6. Switching states implementation of secondary cyclo converter.

switching states of virtual DAB in (2), as seen in Table 3 and Fig. 6, the active vectors are different during the positive and negative v_s, and the zero duty cycle is unequally divided into five parts.

In summary, by incorporating HF chopping of the virtual DAB into the SVM of conventional IMC, the proposed SVM can be derived. This presentation on how the proposed method is formed indicates its principles and relationship with the SVM of conventional IMC. Therefore, the implementation is significantly simplified compared to complicated duty cycles calculation of the primary and secondary matrix converters separately, and then to elaborately combine the two parts, such as the SVM of the back-to-back HF ac linked two TPSP matrix converters in [13].

C. OPERATING MODES ANALYSIS

Fig. 7 shows the operating modes of the HF ac linked converter using the proposed SVM, illustrated by the equivalent circuit in Fig. 2. Based on the positive and negative half cycles of HF transformer voltages v_p and v_s, the operation is categorized as 12 modes in one control cycle. In modes 1~6, the polarity is positive, $v_p = V_{dc1}$, and $v_s = V_{dc2}$; in modes 7~12, the polarity is negative, $v_p = -V_{dc1}$, and $v_s = -V_{dc2}$.

Mode 1 ($t_0 - t_1$): In the primary side, switches S'_{v1}, S'_{v2}, S_1, and S_4 are on; the dc-link current I_{dc1} freewheels, leading to $v_p = 0$. In the secondary side, switches S'_{a2}, S'_{b2}, S_5 and S_8 are on, yet no current flows through them because of the off-state switches S'_{a1} and S'_{b1}, consequently, $I_{dc2} = 0$. In this case, the load resistance R_L is powered by the capacitor C_{fo}. As shown in Figs. 5 and 6, the TPSP matrix converter operates at zero state I_8, and the cyclo converter operates at zero state V_4. The durations of both states are $T_s \cdot d_{10}/4$.

Mode 2 ($t_1 - t_2$): S'_{v1} and S'_{a2} are turned off, while S'_{u1} and S'_{a1} are turned on, other switches maintain the same as in mode 1. One consequent change is that grid source voltages $u_{s,u}$ and $u_{s,v}$ are included in the primary side. It can be seen that $v_p = u_{in,uv}$ in this mode. Another noteworthy change is that in the secondary side, switches S'_{v1}, S'_{v2}, S_1, and S_4 transfer the power from primary side to the load resistance R_L, then L_{fo} and C_{fo} are charged through the HF transformer. In addition, from Figs. 5-7, it can be seen that during this interval, the TPSP matrix converter and the cyclo converter operate at active state I_6 and V_1, respectively, and the duration of this mode is $T_s \cdot d'_{21} \cdot d_{11}/2$.

Mode 3 ($t_2 - t_3$): S'_{b2} is turned off, while S'_{b1} is turned on, other switches remain unchanged as in the mode 2. Since neither S'_{a2} or S'_{b2} is on, the inversion stage cannot conduct current, then R_L is again powered by C_{fo}. On the other hand, since no changes happen in the rectifier stage and active-bridge inverter, the primary side of equivalent operating circuit keeps the same as that in mode 2. Accordingly, the value of v_p is also the same. From Figs. 5 and 6, it can be noted that the TPSP matrix converter maintains at active state I_6, while the cyclo converter switches to zero state V_3. The duration of this mode is calculated as $T_s \cdot d'_{20} \cdot d_{11}/2$.

It is noticeable that v_p remains constant in modes 2~3, and due to the HF transformer, v_p has a relatively fixed proportion with v_s. Therefore, v_s also remains constant in the two modes, which can be seen from Figs. 5 and 6.

Mode 4 ($t_3 - t_4$): All the other switches are working as in the mode 3, except S'_{w2} and S'_{v2}. As a result, $u_{s,v}$ is displaced by $u_{s,w}$ as one of the power sources, which leads to $v_p = u_{in,uw}$. For the secondary side, C_{fo} continues to power R_L, since no changes in the inversion stage and active-bridge rectifier compared to mode 3. Seen from Figs. 5 and 6, the TPSP matrix converter starts to operate at active state I_1, while the cyclo converter continues operating at zero state V_3. The duration of this mode can be written as $T_s \cdot d'_{20} \cdot d_{12}/2$ from the calculation.

Mode 5 ($t_4 - t_5$): The primary side works same as the mode 4. The secondary side returns to the operating state as the mode 2 due to the reversal of switching signals S'_{a1} and S'_{a2}. Seen from Figs. 5 and 6, the TPSP matrix converter still operates at I_1, while the cyclo converter recovers to V_1. The duration of this mode is $T_s \cdot d'_{21} \cdot d_{12}/2$.

Note that v_p and v_s remain constant in modes 4 and 5, and the duty cycle ratio between mode 4 and mode 5 is d'_{20}: d'_{21}, which is similar to that of modes 2 and 3.

Mode 6 ($t_5 - t_6$): In the primary side, switching signals S'_{u1} and S'_{w1} are changed, which makes $v_p = 0$. In the secondary side, the switching signals S'_{a1} and S'_{a2} changes; consequently, the on-off states of all switches are the same as that in mode 1. Figs. 5 and 6 show that the operating states of TPSP matrix converter and cyclo converter are I_9 and V_4, respectively, and the duration of this mode is $T_s \cdot d_{10}/4$.

Modes 7~12 ($t_6 - t_{12}$): In these modes, the switches states of the equivalent IMC correspond to those in modes 6~1, while the states of virtual DAB are opposite. In addition,
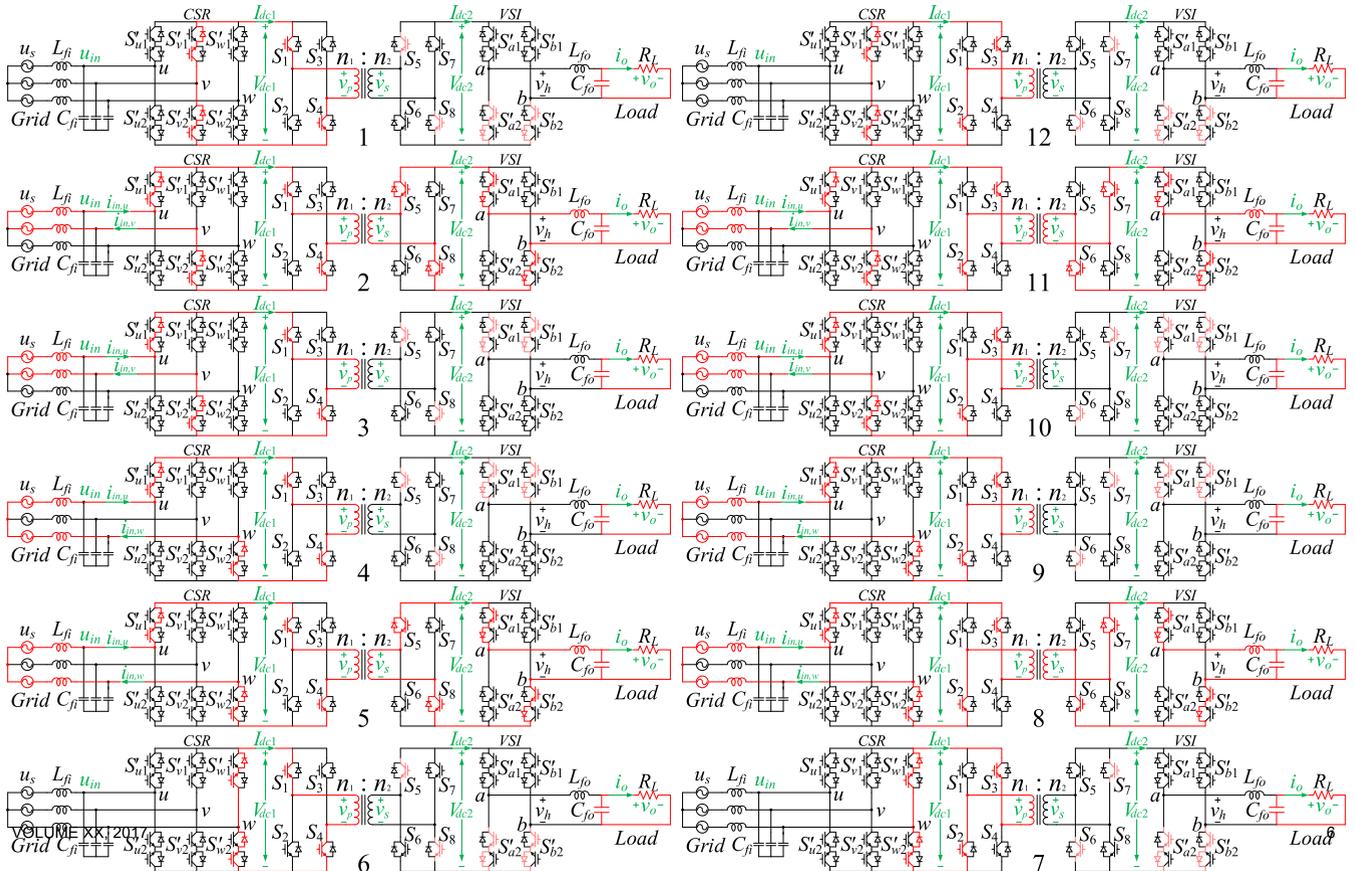
FIGURE 7. Operating modes of the HF ac linked converter with proposed SVM.

as shown in Figs. 5 and 6, the durations of modes 7~12 are equal to the durations of modes 6~1.

D. VOLTAGE GAIN ANALYSIS

From the proposed SVM, the average voltage of primary virtual dc link is [36]

$$\bar{V}_{dc1} = \frac{3}{2} M_1 U_{sm} cos\varphi_i \qquad (7)$$

where U_{sm} denotes the amplitude of three-phase voltage u_s and φ_i denotes the power factor angel of three-phase side.

With (3) and $\bar{V}_{dc2} = (n_2/n_1)\bar{V}_{dc1} = n\bar{V}_{dc1}$, the amplitude of output voltage v_o is obtained by

$$V_{om} = \frac{3}{4} n M_1 M_2 U_{sm} cos\varphi_i \qquad (8)$$

IV. SIMULATION AND HARDWARE-IN-LOOP INVESTIGATIONS

The proposed SVM method for the HF ac linked converter of Fig. 1 is simulated in MATLAB/Simulink and implemented in the RT-BOX HIL platform. The system specifications are as follows: the root-mean-square (RMS) voltage of three-phase side grid is 380 V; the fundamental frequency f_0 of three-phase side grid is 50 Hz; the switching frequency is 10 kHz; the three-phase side filter inductance L_{fi} and

capacitance C_{fi} are 2 *m*H and 100 μF, respectively; and the output filter inductance L_{fo} and capacitance C_{fo} are 2 *m*H and 10 μF at the single-phase load, and 1 *m*H and 100 μF at the dc load, respectively.

In the HIL implementation, the TPSP matrix converter and single-phase cyclo converter formed HF ac linked converter circuit is built in the RT-BOX, the proposed SVM is programmed in the TMS320F28069 digital signal processor (DSP) [11]. The DSP generated switching signals based on the SVM are transferred to the converter circuit in the RT-BOX, through the pulse width modulation (PWM) ports of DSP and digital input ports of the RT-BOX. The power flow from three-phase 380 V/50 Hz ac grid to single-phase 120 V/60 Hz ac load and 400 V dc load are investigated, respectively. Simulation and HIL results are shown in Figs. 8-13.

A. 120 V/60 HZ SINGLE-PHASE AC LOAD

From (8), the $n_1 : n_2 = 1 : 1$ is applied to the HF transformer; the modulation index of rectifier and inversion stages are $M_1 = 0.8$ and $M_2 = 0.82$, respectively, of the equivalent IMC. A $R_L = 15$ Ω is applied in the single-phase ac load. Figs. 8 and 9 show simulation and HIL results, respectively, of three-phase input voltages of primary TPSP matrix
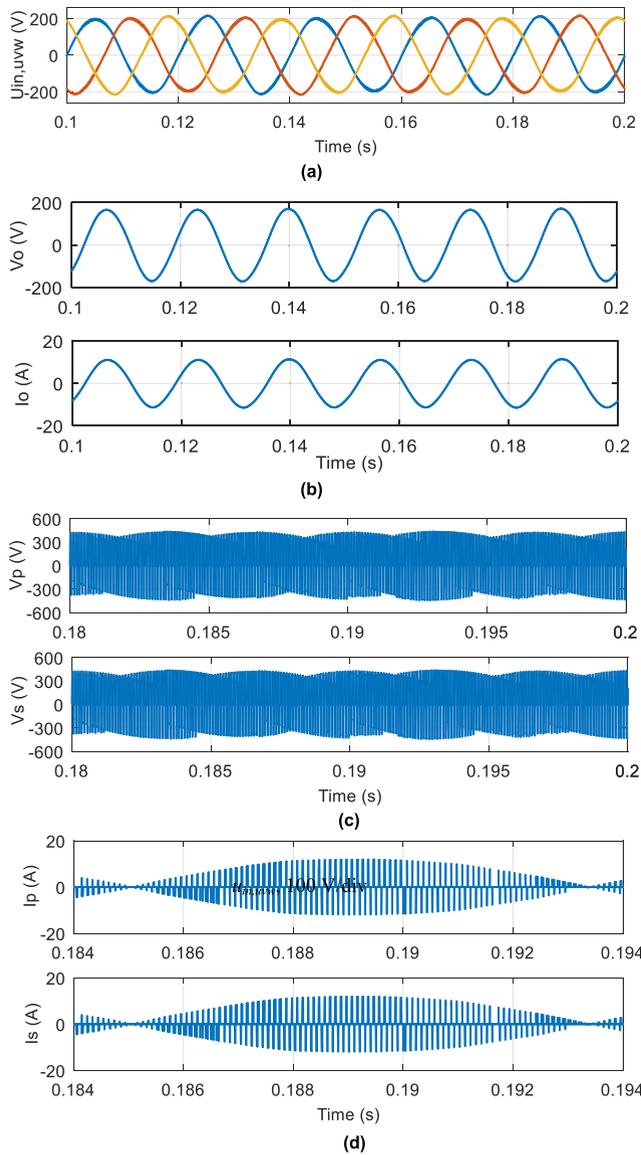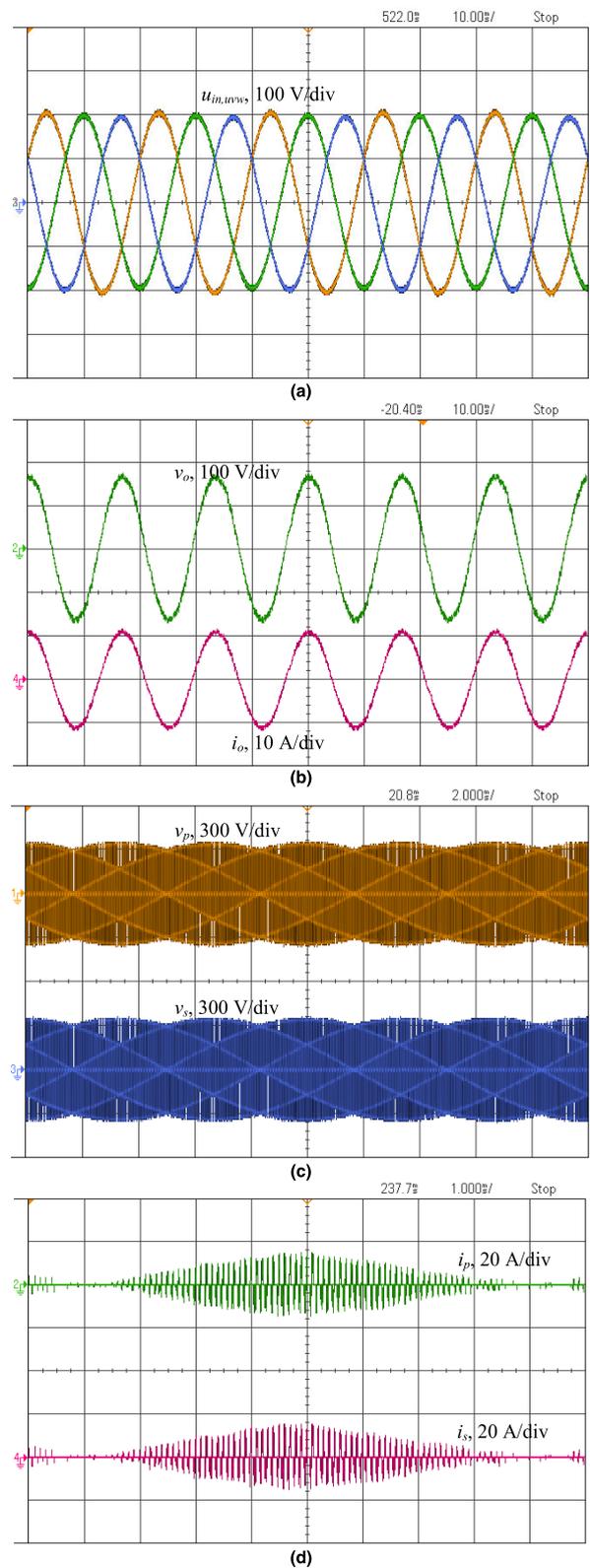
FIGURE 8. Simulation results of 120 V/60 Hz single-phase ac load. (a) Three-phase input voltages of primary TPSP matrix converter; (b) single-phase load voltage and current; (c) primary and secondary voltages of the HF transformer; and (d) primary and secondary currents of the HF transformer.

FIGURE 9. HIL results of 120 V/60 Hz single-phase ac load. (a) Three-phase input voltages of primary TPSP matrix converter; (b) single-phase load voltage and current; (c) primary and secondary voltages of the HF transformer; and (d) primary and secondary currents of the HF transformer.

converter, single-phase load voltage and current, as well as primary and secondary voltages and currents of the HF transformer. Fig. 10 shows Fast Fourier Transform (FFT) analysis of the TPSP matrix converter input voltage and load current.

From Figs. 8 (a) and (b) and 9 (a) and (b), it can be seen that with the proposed SVM, the 380 V/50 Hz three-phase ac voltage is converted to the 120 V/60 Hz single-phase ac voltage through the HF ac linked TPSP matrix converter and cyclo converter.

The load current is sinusoidal with low harmonics, which has the total harmonic distortion (THD) of 1.71%, as shown in Fig. 10 (b). The low distortion is also achieved for the TPSP
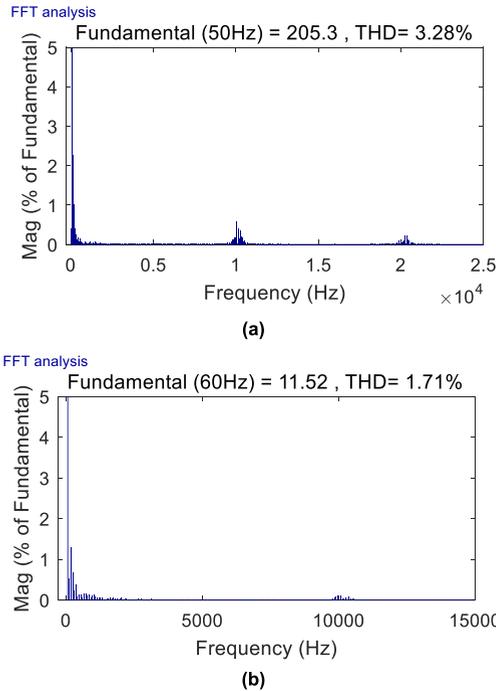
FIGURE 10. FFT analysis of the (a) input voltage u_{in} and (b) output current i_o at 120 V/60 Hz single-phase ac load.

matrix converter input voltage, as seen from the 3.28% THD in Fig. 10 (a).

From Figs. 8 (c) and (d) and 9 (c) and (d), it can be seen that the amplitudes of primary and secondary voltages of the HF transformer are equal to each other; the same to the primary and secondary currents. They match the 1:1 turns ratio of the transformer.

B. 400 V DC LOAD

To supply a 400-V dc load, the $n_1 : n_2 = 2 : 3$ is applied to the HF transformer; the $M_1 = 0.8$ and $M_2 = 0.75$ are performed to the inversion and conversion-stage modulation indexes, respectively, according to (8). The dc load is at $R_L = 40\ \Omega$.

Simulation and HIL results of circuit waveforms are shown in Figs. 11 and 12. Fig. 13 shows FFT analysis of TPSP matrix converter input voltages and dc load current.

From Figs. 11 (b) and 12 (b), it can be seen that the 400 V dc voltage is obtained for the dc load, with the peak-to-peak ripple ratio within 5% of the average output voltage. As a result, the load current is also low ripple, as the 2.57% ratio to the dc component shown in Fig. 13 (b). From Figs. 11 (c) and (d) and 12 (c) and (d), the amplitude ratio of primary and secondary voltages of the HF transformer matches the 2:3 turns ratio.

C. DISCUSSIONS

From Figs. 8, 9, 11, and 12, it can be seen that the voltage amplitude and frequency conversion are fulfilled using the proposed SVM. In addition, there are ripples doubling
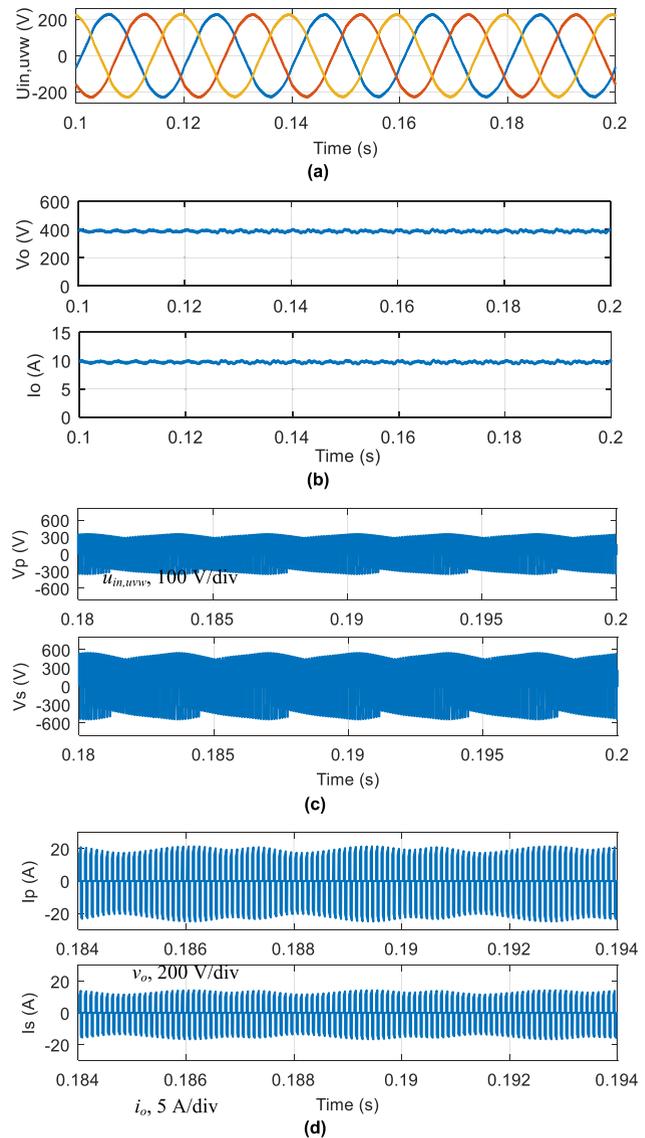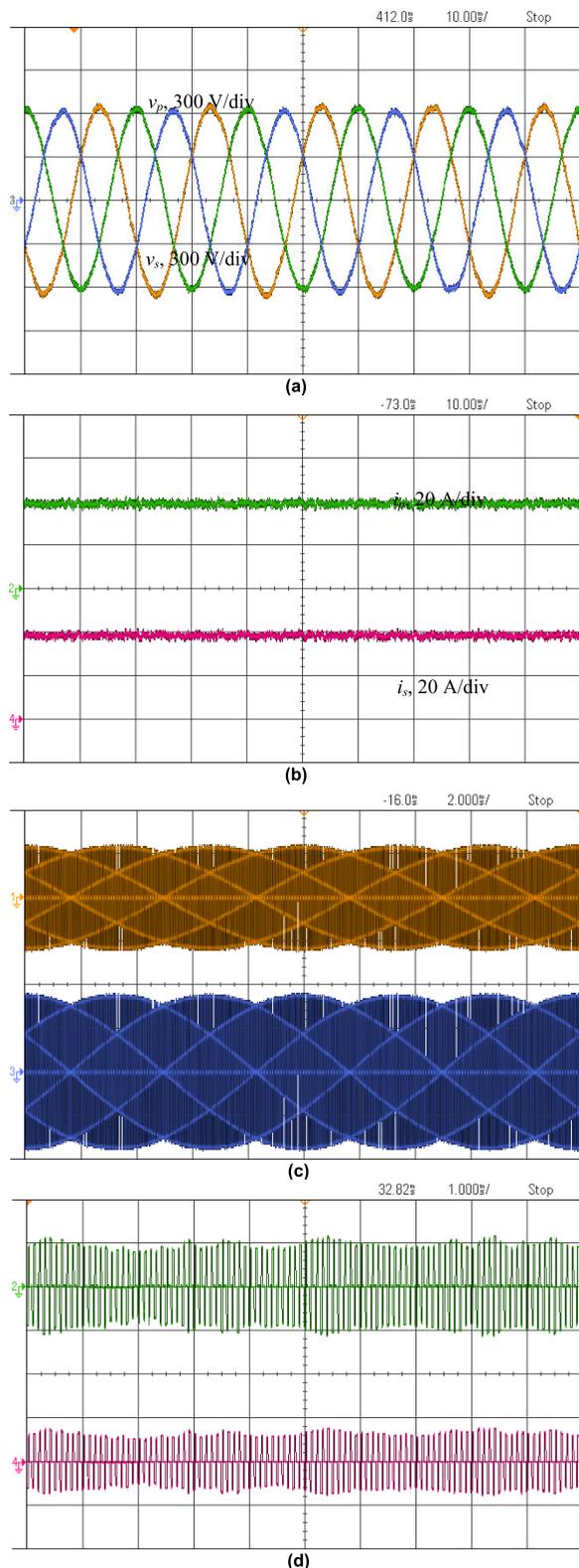

FIGURE 11. Simulation results of dc load. (a) Three-phase input voltages of primary TPSP matrix converter; (b) dc load voltage and current; (c) primary and secondary voltages of the HF transformer; and (d) primary and secondary currents of the HF transformer.

the output 60 Hz frequency in the primary and secondary currents when the cyclo converter outputs single-phase ac. Low-frequency ripple appears in the primary and secondary voltages of the HF transformer as well. Those low-frequency voltage and current ripples cause unwanted low-order harmonics in the input voltages and output current, as seen in Figs. 10 and 13.

Compensating circuit through paralleling a bidirectional switch in each of the three phases with a series inductor has been developed for traditional TPSP matrix converter [37], [38]. Power decoupling technique of traditional single-phase inverter is investigated in detail through paralleling types of decoupling circuit, such as buck or boost-type converter with a series compensating capacitor, to the dc
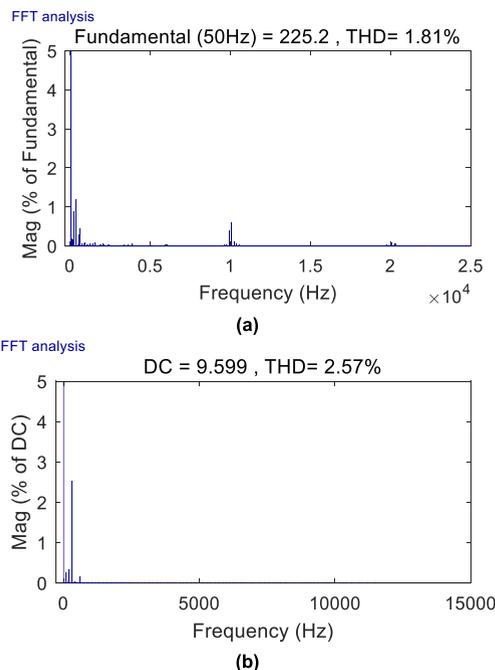
FIGURE 12. HIL results of dc load. (a) Three-phase input voltages of primary TPSP matrix converter; (b) dc load voltage and current; (c) primary and secondary voltages of the HF transformer; and (d) primary and secondary currents of the HF transformer.

FIGURE 13. FFT analysis of the (a) input voltage u_{in} and (b) output current i_o at dc load.

link of the single-phase inverter [44], [45]. Similarly, those techniques can be transplanted to the TPSP matrix converter and single-phase cyclo converter formed smart transformer, due to the inherited topology from the two.
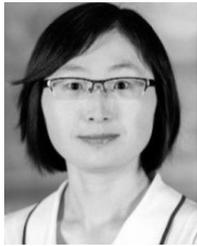
V. CONCLUSION

This paper proposed a simple to implement SVM for the TPSP matrix converter and single-phase cyclo converter formed HF ac linked converter, which can be used to convert between three-phase ac and single-phase ac/dc. The three-phase ac voltages are rectified into virtual dc voltage which is then inverted to HF ac voltage through the primary matrix converter. The virtual dc voltage is regained and then converted to single-phase ac or adjustable dc voltage by the secondary cyclo converter. Based on the equivalent circuit presented, the proposed SVM method was disclosed accordingly through the SVM of traditional IMC taking into considerations of the voltage chopping of HF transformer, voltage and current control of primary and secondary sides, and leakage energy commutation. At the end, simulation and HIL implementation results of different output voltage types verified the proposed method, providing an effective solution for various DGs tied into utility grids.

REFERENCES

[1] J. W. Kolar and G. Ortiz, "Solid-state-transformers: Key components of future traction and smart grid systems," in *Proc. Int. Power Electron. Conf.-ECCE Asia (IPEC)*, 2014, pp. 1–15.

[2] J. Feng, B. Zeng, D. Zhao, G. Wu, Z. Liu, and J. Zhang, "Evaluating demand response impacts on capacity credit of renewable distributed generation in smart distribution systems," *IEEE Access*, vol. 6, pp. 14307–14317, 2018.

[3] J. Hong, J. Yin, Y. Liu, J. Peng, and H. Jiang, "Energy management and control strategy of Photovoltaic/Battery hybrid distributed power generation systems with an integrated three-port power converter," *IEEE Access*, vol. 7, pp. 82838–82847, 2019.

[4] J. E. Huber and J. W. Kolar, "Applicability of solid-state transformers in Today's and future distribution grids," *IEEE Trans. Smart Grid*, vol. 10, no. 1, pp. 317–326, Jan. 2019.

[5] X. Gao, F. Sossan, K. Christakou, M. Paolone, and M. Liserre, "Concurrent voltage control and dispatch of active distribution networks by means of smart transformer and storage," *IEEE Trans. Ind. Electron.*, vol. 65, no. 8, pp. 6657–6666, Aug. 2018.

[6] M. Andresen, K. Ma, G. De Carne, G. Buticchi, F. Blaabjerg, and M. Liserre, "Thermal stress analysis of medium-voltage converters for smart transformers," *IEEE Trans. Power Electron.*, vol. 32, no. 6, pp. 4753–4765, Jun. 2017.

[7] A. Agrawal, C. S. Nalamati, and R. Gupta, "Hybrid DC–AC zonal microgrid enabled by solid-state transformer and centralized ESD integration," *IEEE Trans. Ind. Electron.*, vol. 66, no. 11, pp. 9097–9107, Nov. 2019.

[8] D. Dong, M. Agamy, J. Z. Bebic, Q. Chen, and G. Mandrusiak, "A modular SiC high-frequency solid-state transformer for medium-voltage applications: Design, implementation, and testing," *IEEE J. Emerg. Sel. Topics Power Electron.*, vol. 7, no. 2, pp. 768–778, Jun. 2019.

[9] Z. Zheng, Z. Gao, C. Gu, L. Xu, K. Wang, and Y. Li, "Stability and voltage balance control of a modular converter with multiwinding high-frequency transformer," *IEEE Trans. Power Electron.*, vol. 29, no. 8, pp. 4183–4194, Aug. 2014.

[10] Y. Shi, R. Li, Y. Xue, and H. Li, "High-Frequency-Link-Based grid-tied PV system with small DC-link capacitor and low-frequency ripple-free maximum power point tracking," *IEEE Trans. Power Electron.*, vol. 31, no. 1, pp. 328–339, Jan. 2016.

[11] F. D. Freijedo, E. Rodriguez-Diaz, and D. Dujic, "Stable and passive high-power dual active bridge converters interfacing MVDC grids," *IEEE Trans. Ind. Electron.*, vol. 65, no. 12, pp. 9561–9570, Dec. 2018.

[12] K. Basu and N. Mohan, "A single-stage power electronic transformer for a three-phase PWM AC/AC drive with source-based commutation of leakage energy and common-mode voltage suppression," *IEEE Trans. Ind. Electron.*, vol. 61, no. 11, pp. 5881–5893, Nov. 2014.

[13] K. Basu, A. Shahani, A. K. Sahoo, and N. Mohan, "A single-stage solid-state transformer for PWM AC drive with source-based commutation of leakage energy," *IEEE Trans. Power Electron.*, vol. 30, no. 3, pp. 1734–1746, Mar. 2015.

[14] K. Koiwa, J.-I. Itoh, and M. Shioda, "Improvement of waveform for high frequency AC-linked matrix converter with SVM based on virtual indirect control," in *Proc. IEEE Appl. Power Electron. Conf. Exposit. (APEC)*, Mar. 2015, pp. 3359–3366.

[15] K. Inoue, M. Shioda, M. Katade, A. Goto, S. Morishita, J. Itoh, and K. Koiwa, "Space vector modulation based on virtual indirect control for high frequency AC-linked matrix converter," in *Proc. Int. Power Electron. Conf. (IPEC-Hiroshima-ECCE ASIA)*, May 2014, pp. 130–137.

[16] Y. Liu, Y. Liu, H. Abu-Rub, B. Ge, R. S. Balog, and Y. Xue, "Model predictive control of a matrix-converter based solid state transformer for utility grid interaction," in *Proc. IEEE Energy Convers. Congr. Exposit. (ECCE)*, Milwaukee, WI, USA, Sep. 2016, pp. 1–6.

[17] H. Chen, A. Prasai, and D. Divan, "Dyna-C: A minimal topology for bidirectional solid-state transformers," *IEEE Trans. Power Electron.*, vol. 32, no. 2, pp. 995–1005, Feb. 2017.

[18] H. Chen and D. Divan, "Soft-switching solid-state transformer (S4T)," *IEEE Trans. Power Electron.*, vol. 33, no. 4, pp. 2933–2947, Apr. 2018.

[19] H. Chen and D. Divan, "Design of a 10-kV·A soft-switching solid-state transformer (S4T)," *IEEE Trans. Power Electron.*, vol. 33, no. 7, pp. 5724–5738, Jul. 2018.

[20] K. Mozaffari and M. Amirabadi, "A highly reliable and efficient class of single-stage high-frequency AC-link converters," *IEEE Trans. Power Electron.*, vol. 34, no. 9, pp. 8435–8452, Sep. 2019.

[21] K. Mozaffari and M. Amirabadi, "A versatile family of partial-resonance Inductive-AC-Link universal converters," *IEEE Trans. Power Electron.*, vol. 34, no. 8, pp. 7292–7309, Aug. 2019.

[22] V. Vlatkovic, D. Borojevic, and F. C. Lee, "A zero-voltage switched, three-phase isolated PWM buck rectifier," *IEEE Trans. Power Electron.*, vol. 10, no. 2, pp. 148–157, Mar. 1995.

[23] J. Afsharian, D. Xu, B. Wu, B. Gong, and Z. Yang, "A new PWM and commutation scheme for one phase loss operation of three-phase isolated buck matrix-type rectifier," *IEEE Trans. Power Electron.*, vol. 33, no. 11, pp. 9854–9865, Nov. 2018.

[24] J. Afsharian, D. Xu, B. Wu, B. Gong, and Z. Yang, "The optimal PWM modulation and commutation scheme for a three-phase isolated buck matrix-type rectifier," *IEEE Trans. Power Electron.*, vol. 33, no. 1, pp. 110–124, Jan. 2018.

[25] Y. Hayashi, H. Motoyama, and T. Takeshita, "Wireless power transfer system using three-phase to single-phase matrix converter," in *Proc. Int. Power Electron. Conf. (IPEC-Niigata -ECCE Asia)*, Niigata, Japan, May 2018, pp. 356–362.

[26] M. Wang, Q. Huang, S. Guo, X. Yu, W. Yu, and A. Q. Huang, "Soft-switched modulation techniques for an isolated bidirectional DC–AC," *IEEE Trans. Power Electron.*, vol. 33, no. 1, pp. 137–150, Jan. 2018.

[27] M. A. Sayed, K. Suzuki, T. Takeshita, and W. Kitagawa, "PWM switching technique for three-phase bidirectional grid-tie DC–AC–AC converter with high-frequency isolation," *IEEE Trans. Power Electron.*, vol. 33, no. 1, pp. 845–858, Jan. 2018.

[28] L. Schrittwieser, P. Cortes, L. Fassler, D. Bortis, and J. W. Kolar, "Modulation and control of a three-phase phase-modular isolated matrix-type PFC rectifier," *IEEE Trans. Power Electron.*, vol. 33, no. 6, pp. 4703–4715, Jun. 2018.

[29] L. Schrittwieser, M. Leibl, and J. W. Kolar, "99% efficient isolated three-phase matrix-type DAB buck–boost PFC rectifier," *IEEE Trans. Power Electron.*, vol. 35, no. 1, pp. 138–157, Jan. 2020.

[30] D. Das, N. Weise, K. Basu, R. Baranwal, and N. Mohan, "A bidirectional soft-switched DAB-based single-stage three-phase AC–DC converter for V2G application," *IEEE Trans. Transp. Electrific.*, vol. 5, no. 1, pp. 186–199, Mar. 2019.

[31] U. Nasir, A. Costabeber, P. Wheeler, M. Rivera, and J. Clare, "A three-phase modular isolated matrix converter," *IEEE Trans. Power Electron.*, vol. 34, no. 12, pp. 11760–11773, Dec. 2019.

[32] Y. Liu, J. He, B. Ge, Y. Xue, and S. Bavhan, "General space vector modulation of a high-frequency AC linked universal converter for distributed generations," in *Proc. 44th Annu. Conf. IEEE Ind. Electron. Soc. (IECON)*, Oct. 2018, pp. 5541–5546.

[33] P. W. Wheeler, J. Rodriguez, J. C. Clare, L. Empringham, and A. Weinstein, "Matrix converters: A technology review," *IEEE Trans. Ind. Electron.*, vol. 49, no. 2, pp. 276–288, Apr. 2002.

[34] T. Friedli, J. W. Kolar, J. Rodriguez, and P. W. Wheeler, "Comparative evaluation of three-phase AC–AC matrix converter and voltage dc-link back-to-back converter systems," *IEEE Trans. Ind. Electron.*, vol. 59, no. 12, pp. 4487–4510, Dec. 2012.

[35] B. Ge, Q. Lei, W. Qian, and F. Z. Peng, "A family of Z-source matrix converters," *IEEE Trans. Ind. Electron.*, vol. 59, no. 1, pp. 35–46, Jan. 2012.

[36] S. Liu, B. Ge, Y. Liu, H. Abu-Rub, R. S. Balog, and H. Sun, "Modeling, analysis, and parameters design of LC-filter-integrated quasi-Z-source indirect matrix converter," *IEEE Trans. Power Electron.*, vol. 31, no. 11, pp. 7544–7555, Nov. 2016.

[37] M. Wang, Q. Huang, W. Yu, and A. Q. Huang, "High-frequency AC distributed power delivery system," in *Proc. IEEE Appl. Power Electron. Conf. Exposit. (APEC)*, Long Beach, CA, Mar. 2016, pp. 3648–3654.

[38] Y. Liu, W. Liang, B. Ge, H. Abu-Rub, and N. Nie, "Quasi-Z-source three-to-single-phase matrix converter and ripple power compensation based on model predictive control," *IEEE Trans. Ind. Electron.*, vol. 65, no. 6, pp. 5146–5156, Jun. 2018.

[39] H. Guo, H. Ge, and Y. Xu, "The control strategy of buck-type 3-1 MC under unbalanced input voltage," *IEEE Access*, vol. 6, pp. 6316–6326, 2018.

[40] J. I. Leon, S. Kouro, L. G. Franquelo, J. Rodriguez, and B. Wu, "The essential role and the continuous evolution of modulation techniques for voltage-source inverters in the past, present, and future power electronics," *IEEE Trans. Ind. Electron.*, vol. 63, no. 5, pp. 2688–2701, May 2016.

[41] P. Cortes, G. Ortiz, J. I. Yuz, J. Rodriguez, S. Vazquez, and L. G. Franquelo, "Model predictive control of an inverter with output *LC* filter for UPS applications," *IEEE Trans. Ind. Electron.*, vol. 56, no. 6, pp. 1875–1883, Jun. 2009.

[42] Y. Xia, X. Zhang, M. Qiao, F. Yu, Y. Wei, and P. Zhu, "Research on a new indirect space-vector overmodulation strategy in matrix converter," *IEEE Trans. Ind. Electron.*, vol. 63, no. 2, pp. 1130–1141, Feb. 2016.

[43] Y. Liu, B. Ge, H. Abu-Rub, and F. Z. Peng, "An effective control method for quasi-Z-source cascade multilevel inverter based grid-tie single-phase photovoltaic power system," *IEEE Trans. Ind. Informat.*, vol. 10, no. 1, pp. 399–407, Feb. 2014.

[44] H. Zhang, X. Li, B. Ge, and R. S. Balog, "Capacitance, DC voltage utilizaton, and current stress: Comparison of double-line frequency ripple power decoupling for single-phase systems," *IEEE Ind. Electron. Mag.*, vol. 11, no. 3, pp. 37–49, Sep. 2017.

[45] Y. Liu, B. Ge, H. Abu-Rub, and F. Blaabjerg, "Single-phase Z-source/quasi-Z-source inverters and converters: An overview of double-line-frequency power-decoupling methods and perspectives," *IEEE Ind. Electron. Mag.*, vol. 12, no. 2, pp. 6–23, Jun. 2018.

XIAO LI (Member, IEEE) received the B.Sc. degree in automation from the Harbin Institute of Technology (HIT), China, in 2012, and the Ph.D. degree in electrical engineering from the Department of Electrical and Computer Engineering, Texas A&M University, College Station, TX, USA.

His research interests include power electronics system integration, distributed generations, general power electronic circuit topologies, modeling and control, and wide bandgap devices.

YUSHAN LIU (Senior Member, IEEE) received the B.Sc. degree in automation from the Beijing Institute of Technology, Beijing, China, in 2008, and the Ph.D. degree in electrical engineering from the School of Electrical Engineering, Beijing Jiaotong University, Beijing, in 2014.

She was a Postdoctoral Fellow and an Assistant Research Scientist with the Department of Electrical and Computer Engineering, Texas A&M University at Qatar, Doha, Qatar, from 2014 to 2017. She is currently an Associate Professor with the School of Automation Science and Electrical Engineering, Beihang University, Beijing. She has published more than 70 journal and conference papers, one book, and one book chapter in the area of expertise. Her research interests include impedance source inverters, cascade multilevel converters, photovoltaic power integration, renewable energy systems, model predictive control, and smart transformers.

Dr. Liu received the Research Fellow Excellence Award from Texas A&M University at Qatar, the Excellent Doctoral Dissertations Prize from Beijing Jiaotong University. She is also an Associate Editor of the IEEE Transactions on Industrial Electronics and IEEE Open Journal of Industrial Electronics Society.

YAOSUO XUE (Senior Member, IEEE) received the B.Sc. degree in electrical engineering from East China Jiaotong University, Nanchang, China, in 1991, and the M.Sc. degree in electrical engineering from the University of New Brunswick, Fredericton, Canada, in 2004.

From 1991 to 2000, he was an Electrical Engineer-in-Charge with China Railway Design Corporation and led the traction power systems Research and Development of the first China's high-speed railway. From 2005 to 2006, he was with Capstone Turbine Corporation as a Lead Power Electronics and a Systems Engineer. From 2006 to 2008, he was a NSERC PGS-Doctor Scholar with the University of New Brunswick. He was with Siemens Corporate Research from 2009 to 2015 and established Corporate Technology USA power electronics program. He is currently with the Oak Ridge National Laboratory. His research interests include multilevel converters and smart inverter controls for renewable energy and utility applications. He is also an Associate Editor of the IEEE Transaction on Power Electronics and the IEEE Journal of Emerging and Selected Topics in Power Electronics.

JIE HE was born in Fuyang, China, in 1996. He received the B.Sc. degree in electrical engineering from the School of Automation Science and Electrical Engineering, Beihang University, Beijing, China, in 2018, where he is currently pursuing the M.Sc. degree in electrical engineering.

His research interests include ac-ac power conversion, pulse-width modulation, silicon carbide devices, and its applications in power converter.

FREDE BLAABJERG (Fellow, IEEE) received the Ph.D. degree in electrical engineering from Aalborg University, in 1995.

He was with ABB-Scandia, Randers, Denmark, from 1987 to 1988. He became an Assistant Professor in 1992, an Associate Professor in 1996, and a Full Professor of power electronics and drives in 1998. Since 2017, he became a Villum Investigator. He has published more than 500 journal articles in the fields of power electronics and its applications. He is the coauthor of two monographs and editor of seven books in power electronics and its applications. His current research interests include power electronics and its applications such as in wind turbines, PV systems, reliability, harmonics, and adjustable speed drives. He received 24 IEEE Prize Paper Awards, the IEEE PELS Distinguished Service Award in 2009, the EPE-PEMC Council Award in 2010, the IEEE William E. Newell Power Electronics Award 2014, and the Villum Kann Rasmussen Research Award 2014. He has been a Distinguished Lecturer of the IEEE Power Electronics Society, from 2005 to 2007, and of the IEEE Industry Applications Society, from 2010 to 2011 and from 2017 to 2018. In 2018, he is also the President-Elect of IEEE Power Electronics Society. He is nominated in 2014, 2015, 2016, and 2017 by Thomson Reuters to be between the most 250 cited researchers in Engineering in the world. In 2017, he became a Honoris Causa at University Politehnica Timisoara (UPT), Romania. He was the Editor-in-Chief of the IEEE Transactions on Power Electronics, from 2006 to 2012.

BAOMING GE (Member, IEEE) received the Ph.D. degree in electrical engineering from Zhejiang University, Hangzhou, China, in 2000.

He was with the Department of Electrical Engineering, Tsinghua University, Beijing, China, from 2000 to 2002. In 2002, he joined the School of Electrical Engineering, Beijing Jiaotong University, Beijing, and was promoted to a Professor, in 2006. He was with the University of Coimbra, Coimbra, Portugal, from 2004 to 2005, and with Michigan State University, East Lansing, MI, USA, from 2007 to 2008 and 2010 to 2014. Then, he joined the Department of Electrical and Computer Engineering, Texas A&M University, College Station, TX, USA. He has authored more than 200 journal and conference papers, two books, two book chapters, and holds seven patents. His main research interests are the renewable energy generation, electrical machine drives, and power electronics.

● ● ●